Int. J. Electrochem. Sci., 13 **(2018)** 10101 – 10112, doi: 10.20964/2018.11.42

International Journal of
ELECTROCHEMICAL
SCIENCE
www.electrochemsci.org

Enhanced Electrochemical Reduction of CO_2 to Ethylene on Electrodeposited Copper in 0.1 M $KHCO_3$

Tian Qin[1,2,3], *Yao Qian*[2], *Fan Zhang*[2], *Anqi Chen*[2], *Bolin Lin*[2,*]

[1] Shanghai Institute of Microsystem and Information Technology, Chinese Academy of Sciences, Shanghai 200050, P. R. China.
[2] School of Physical Science and Technology, ShanghaiTech University, Shanghai 201210, P. R. China.
[3] University of Chinese Academy of Sciences, Beijing 100049, China.
[*]E-mail: linbl@shanghaitech.edu.cn

Received: 6 June 2018 / *Accepted:* 2 August 2018 / *Published:* 1 October 2018

Copper dendritic structures with low porosity were prepared via electrodeposition under acid-free conditions. The microstructure (morphology and facet selectivity) could be tuned by altering the electrodeposition potential and time length. In contrast to previous electrodeposited copper under acidic conditions, the present copper electrodes led to enhanced formation of ethylene relative to polycrystalline copper for electrochemical reduction of carbon dioxide. The synergy of the non-porous dendritic structures and the increased content of exposed high-index crystal facet (311) may account for this improvement.

Keywords: CO_2 reduction; electrocatalysis; copper dendrites; electrodeposition; faradaic efficiency

1. INTRODUCTION

Although considered as a greenhouse gas, CO_2 can also serve as an abundant C1 feedstock for chemicals and fuels [1, 2]. The electrochemical reduction of carbon dioxide using renewable energy is a promising strategy to reduce carbon footprint and mitigate the greenhouse effect [3, 4]. Carbon dioxide can be converted to liquid products (formic acid, methanol, ethanol, etc.) as well as gaseous products (carbon monoxide, methane, ethylene, etc.) as an abundant carbon source [5]. Liquid products are difficult for separation and purification due to dissolution in aqueous solution. Of the gaseous products, ethylene is widely used as an important chemical raw material and is one of the largest chemical products in the world. Currently, only copper-based materials [6-9], nickel gallium alloys [10] and nitrogen-doped graphene quantum dots [11] exhibit high selectivity of converting carbon dioxide to ethylene among the many electrode materials that have been studied. The advantages of copper include cheapness and availability as well as convenience to synthesize various novel architectures [12-15].

Different approaches to various surface morphologies of copper electrodes have been shown to affect the product selectivity for the electrochemical reduction of carbon dioxide. Smooth polycrystalline copper surfaces led to a mixture of ethylene, carbon monoxide and methane [7]. Carbon monoxide and formic acid were mainly generated on heat-annealed copper electrode exhibiting a rod-shaped array of several hundred nanometers in diameter [16]. Oxygen plasma treated copper electrode with micron-sized wires on the surface significantly enhanced the yield of ethylene [9]. Electrochemically roughened electrode with surface covered with 50-100 nm copper nanoparticles resulted in higher selectivity of ethylene and carbon monoxide relative to polycrystalline copper [17].

Electrodeposition is an attractive method to generate deposits tightly adhered to the substrate surface [18]. The structures of the deposited materials can be conveniently tuned by varying the potential, current, electrodeposition time length and concentration of the electrolyte. It has been shown that addition of acid in the electrolytic solution generated hydrogen bubbles as a soft template for the formation of porous copper foams [19-21]. However, open pores of the foams presumably trap ethylene during the electrocatalytic reductions and prolong its residence time, resulting in further hydrogenation of ethylene to less valuable ethane [12, 22, 23]. As such, the reported highest faradaic efficiency of ethylene using electrodeposited copper foam catalysts is ca. 20%, even lower than that of polycrystalline copper [7,23].

In this contribution, we report the first study of the electrochemical reduction of CO_2 to ethylene using copper dendrites prepared via electrodeposition under acid-free conditions as the catalysts. In contrast to the reduction using the soft-template method with acids [12, 20, 22, 23], faradaic efficiencies for the production of ethylene higher than the polycrystalline copper were observed.

2. EXPERIMENTAL

2.1. Fabrication of a copper dendritic structure via electrodeposition

Table 1. New copper electrodes prepared via electrodeposition in an aqueous solution of copper sulfate

Copper electrodes	Electrodeposition potential /(V vs. Ag/AgCl)	Electrodeposition time/s
I	−0.02	60
II	−0.05	60
III	−0.1	60
IV	−0.5	60
V	−1	60
VI	−2	60
VII	−4	60
VIII	−2	0

X	−2	15
XI	−2	30
XII	−2	45

The working area of a polycrystalline copper foil (0.127mm thick, Alfa Aesar, annealed, 99.9% metals basis) was set as 3 cm^2. Prior to the electrodeposition, the electrode was mechanically polished with a sandpaper (800G and 1200G, Matador) to remove the oxide layer, rinsed by deionized water, and then blown by a N_2 flow to eliminate the copper scales on the surface. Finally it was electrically polished in 85% phosphoric acid (Sinopharm Chemical Reagent Co. Ltd.) at a 2.1 V.

We fabricated new copper electrodes via constant-potential electrodeposition with varied potentials and time lengths in 0.1 M $CuSO_4$ (Sinopharm Chemical Reagent Co. Ltd.) aqueous solution （pH=4.0） at 25℃ (Table 1). Cu^{2+} cation in the solution was reduced to produce Cu^0 deposits on the cathode surface with different microstructures by applying different electrodeposition conditions. The dissolution of the polycrystalline copper as a sacrificed anode kept Cu^{2+} cation concentration in the bath constant. Ag/AgCl electrode served as the reference electrode.

2.2. Material characterization

Scanning electron microscopy (SEM, Phenom Prox, Phenom-World; JSM 7800F) and X-ray diffractometer (XRD, Bruker D8 Advance, Cu Kα, 40 kV, 40 mA) were employed to characterize the surface. X-ray photoelectron spectra were obtained using ThermoFisher ESCA 250XI with Al-Ka X-ray source.

2.3. Electrochemical reduction of CO_2

Carbon dioxide (Shanghai Youjiali Gas, ≥99.995%) reduction was carried out in a custom-made electrochemical cell with two compartments separated by an anion exchange membrane (Selemion AMV, AGC Inc.). Platinum mesh (Wuhan gaossunion Technology Co., Ltd., 99.99%) and Ag/AgCl electrode (3.0 M KCl, CH instruments Inc.) served as a counter electrode and a reference electrode, respectively. The controlled-potential electrolysis was performed in CO_2-saturated 0.1 M $KHCO_3$ aqueous solution (pH=6.8) by an electrochemical analyzer (CHI760e, CH instruments Inc.). The gaseous products are purged out of the cell by a continuous flow of CO_2 at a rate of 20 sccm regulated by mass flow controllers (MC-100SCCM-D, Alicat Scientific) for both compartments. After 600 seconds' electrolysis, the gaseous sample was collected by a gas sampling bag and then quantified when completion of the electrolysis by a gas chromatography (GC, Trace 1300, ThermoFisher Scientific) equipped with two thermal conductivity detectors (TCDs) and one flame ionization detector (FID) to detect H_2, CO and hydrocarbons. The GC data collected were used for the determination of the faradaic efficiencies. Calibration of the GC using standard gas mixtures (Shanghai Weichuang Standard Gas Analytical Technology Co., Ltd.) was done for quantification of gaseous samples.

3. RESULTS AND DISCUSSION

The relationship between the faradaic efficiency of ethylene and applied potentials was first probed for commercial polycrystalline Cu electrode as a control sample. Controlled-potential electrolysis was carried out for 650 seconds across a wide potential window (from −1.4 V to −1.9 V vs. Ag/AgCl).

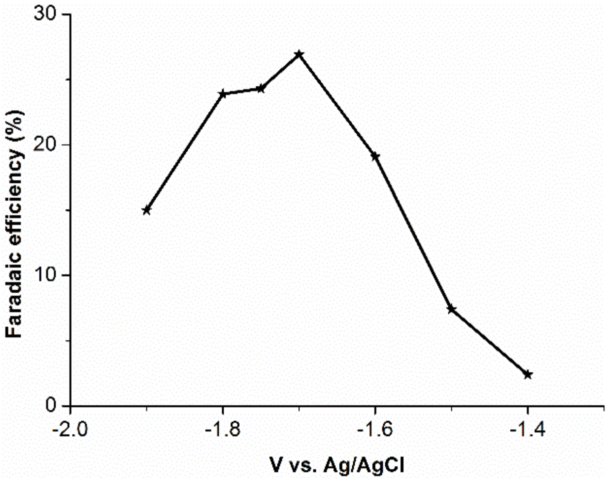

Figure 1. Faradaic efficiency of ethylene as a function of potential in 0.1 M $KHCO_3$.

As shown in Figure 1, the result is consistent with previous reported data in the literature [7]. As the overpotential increased, the faradaic efficiency of ethylene gradually increased until reaching its maximum at −1.7 V vs. Ag/AgCl. The maximal faradaic efficiency of ethylene was 26%.

Copper electrodes with different morphologies were prepared via the electrodeposition process under the acid-free condition. (Table 1) Electrodeposition parameters, such as the applied potentials, have been reported to have a significant effect on the morphology [19, 24]. The relationship between the potential applied and the morphology of the copper deposits was probed under present conditions. Figure 2 showed the SEM images of these copper electrodes via electrodeposition at different potentials. Due to the absence of H_2 bubbles during the electrodeposition in the soft-template method [19], no mesoporous copper foam was observed under the acid-free conditions. Electrodes (a)-(c) displayed a quite rough and porous surface at relatively small potentials (−0.02 V, −0.05 V& −0.1 V). Nanoparticles with ~200 nm size were formed at intermediate deposition potentials (−0.5 V, −1 V). The deposits displayed a characteristic morphology of sporadic dendrites only at −2 V, while a dense layer of precipitates were observed at −4 V. The formation of dendrites might be attributed to the limited mass transfer of metal ions at high deposition potentials [23].

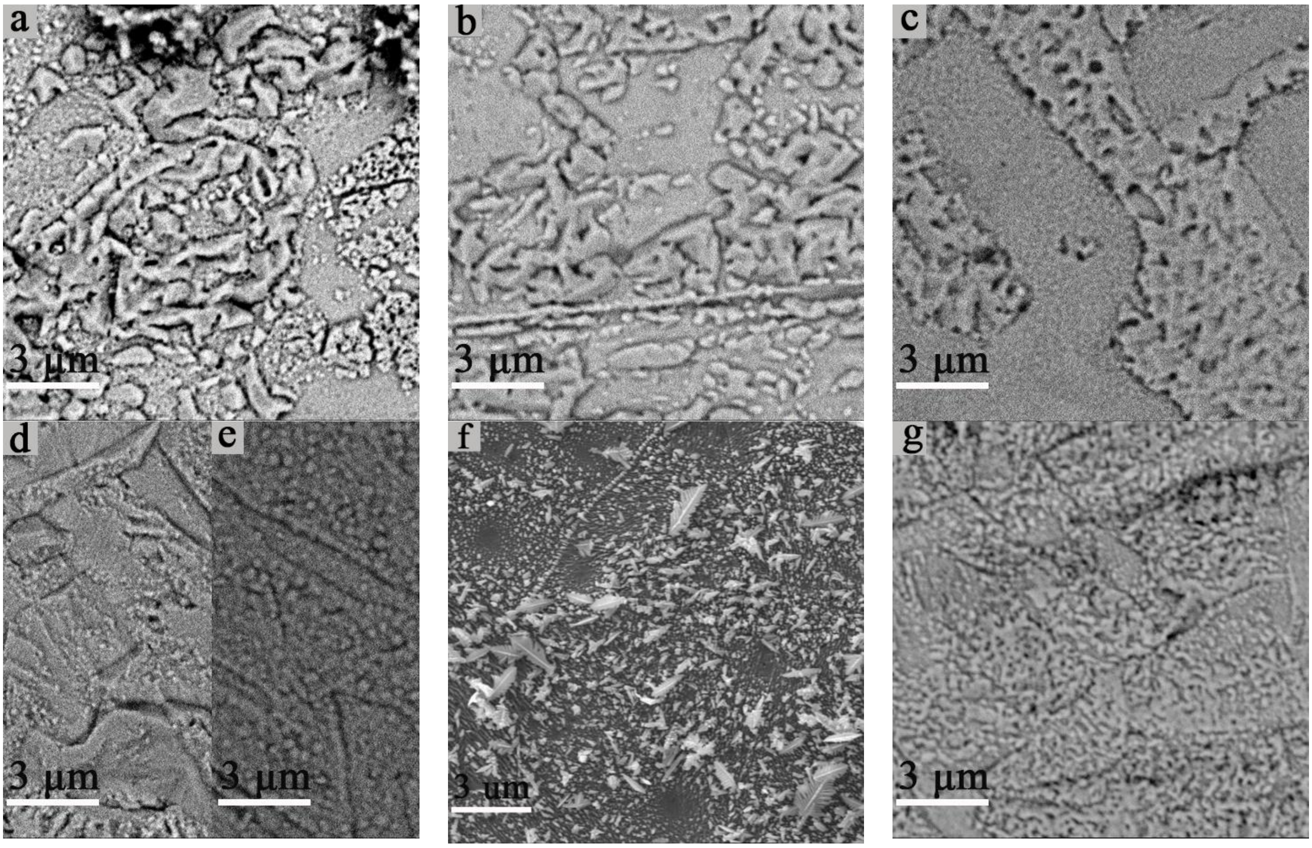

Figure 2. SEM images of copper electrodes deposited at different potentials for 60 seconds. a (−0.02 V); b (−0.05 V); c(−0.1 V); d (−0.5 V); e (−1 V); f (−2 V); g (−4 V). (Scale bar: 3 μm)

Since the control Cu electrode showed the highest faradaic efficiency for the formation of ethylene at −1.7 V vs Ag/AgCl, all the copper electrodes obtained via the electrodeposition were next subjected for carbon dioxide reduction reaction at the same potential to probe the effect of the morphology onto the selectivity for the formation of ethylene. As shown in Figure 3, most electrodes exhibited ethylene faradaic efficiency of ca. 15%, lower than that of the control sample. However, the one covered with dendrites on the surface is the only exception, showing a selectivity for ethylene formation of ca. 32%. And also on the same copper electrode VI, the peak faradaic efficiency for H_2 was achieved at ca. 43%. All the copper electrodes led to CO evolution with a low faradaic yield. For the copper electrode III, CH_4 gained the highest faradaic efficiency of ca. 30%.

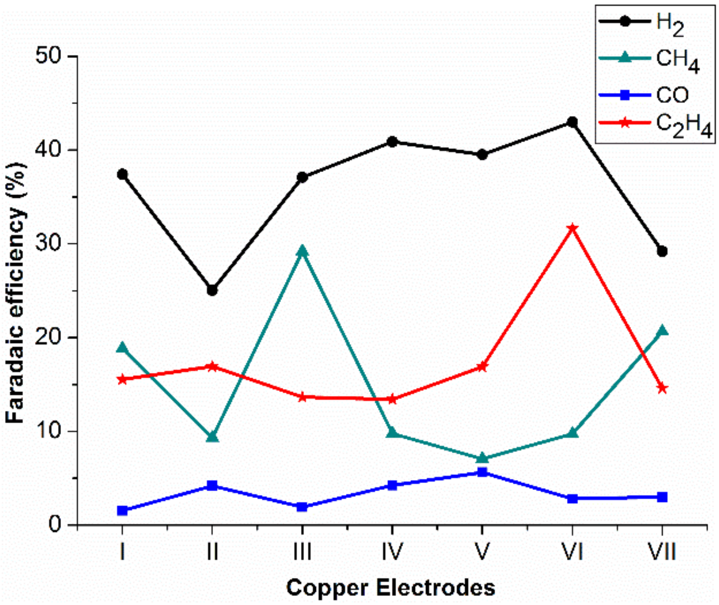

Figure 3. Faradaic efficiency of gaseous products on different electrodes deposited with varied potentials at −1.7 V vs Ag/AgCl in 0.1 M $KHCO_3$.

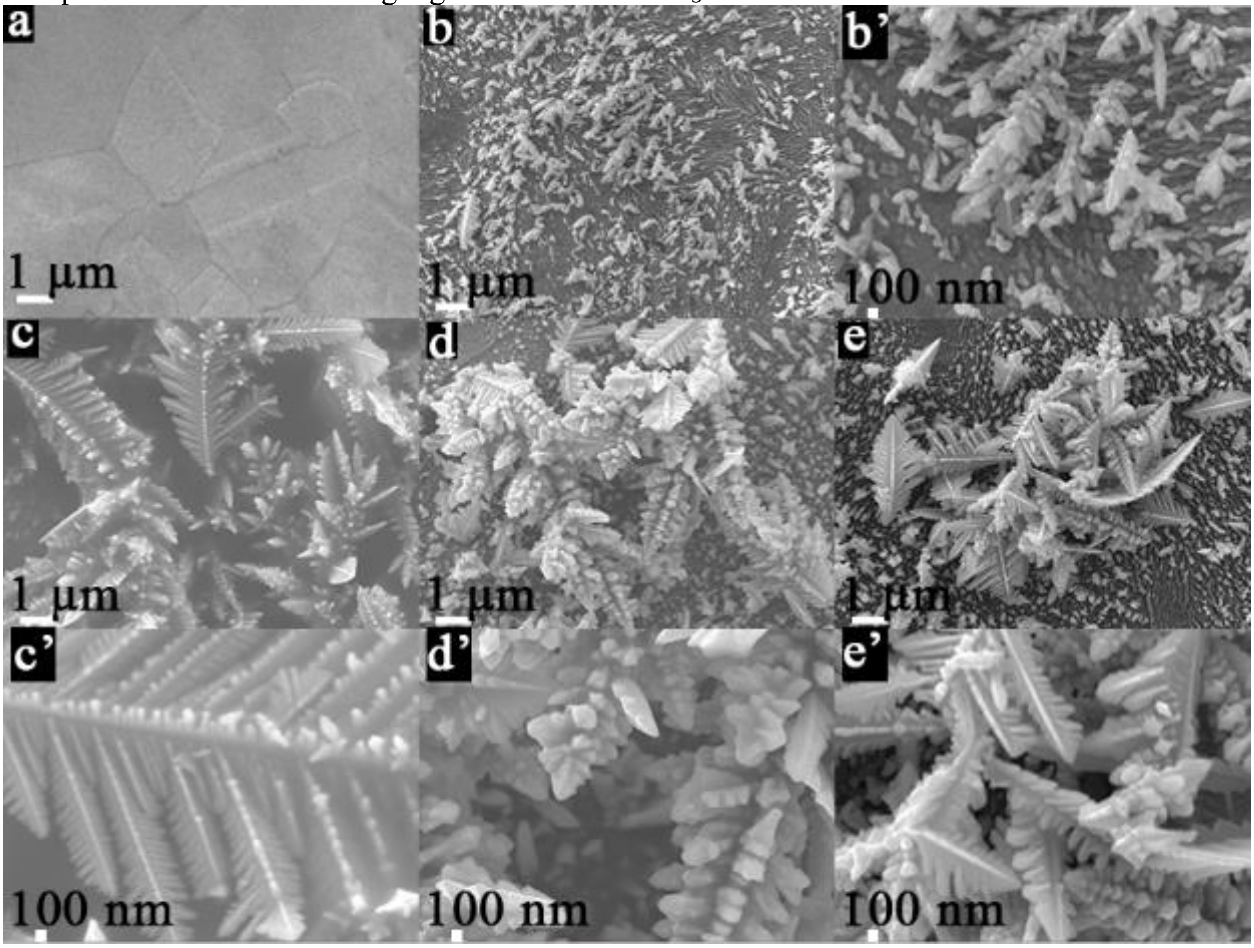

Figure 4. SEM images of copper electrodes deposited at −2 V vs. Ag/AgCl under different time lengths. a (0 s);b (15 s); c (30 s); d (45 s); e (60 s) (Scale bar: 1 μm) and the corresponding b' (15 s); c' (30 s); d '(45 s); e' (60 s) (Scale bar: 100 nm) with higher magnification .

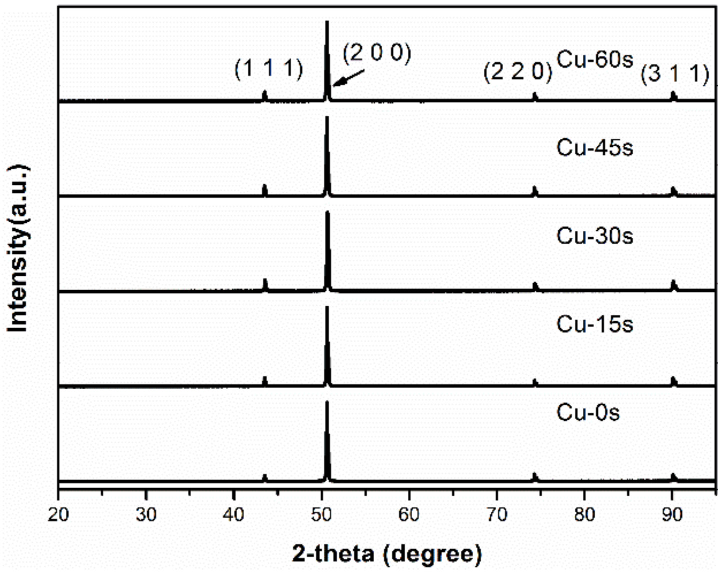

Figure 5. XRD patterns of Cu electrodes deposited at −2 V under different time length.

Since copper dendrites appeared to promote the formation of ethylene, we further probed various different dendrites obtained by changing the deposition time length at the same potential. Figure 4 showed representative SEM images of the copper surfaces after electrodeposition at −2 V vs Ag/AgCl for different lengths of time. Dendritic structures started to appear after a 15-second deposition. Dendrites grew larger and became dense on the electrode surface with increased deposition time length. The obtained surface morphology of the electrodes was not uniform, exhibiting both long and short dendrites with length ranging from sub-100 nm to several microns.

Table 2. The Cu (3 1 1)/(2 0 0) intensity ratio under different lengths of electrodeposition time

Electrodeposition time /s	Cu (3 1 1)/(2 0 0) intensity ratio /(a.u.)
0	0.094
15	0.118
30	0.136
45	0.116
60	0.124

Figure 5 presented the XRD patterns of the copper electrode under different deposition time lengths. Copper crystal facets corresponding to (1 1 1), (2 0 0), (2 2 0), and (3 1 1) were observed. We analyzed the diffraction intensity ratio of (3 1 1) to the main peak (2 0 0) as a function of deposition time length. As shown in Table 2, the ratio of (3 1 1) to (2 0 0) crystal facets increased as the deposition time increased from 0 to 30 seconds and then decreased slightly for further increased deposition time.

As shown in Figure 6 (a), electron binding energies for Cu $2p_{1/2}$ and $2p_{3/2}$ of a representative dendritic sample were 952.3 eV and 932.5 eV, respectively. These binding energies are close to those of soft-template Cu foam [12], suggesting that the copper materials obtained under different deposition conditions had similar electronic structures. The corresponding Cu LMM Auger spectrum (Figure 6 (b)) indicates the presence of both Cu^0 (568.1 eV) and Cu_2O (570.1 eV) on the electrode surface [25]. The existence of Cu_2O was also observed for a foamed Cu electrode[23].

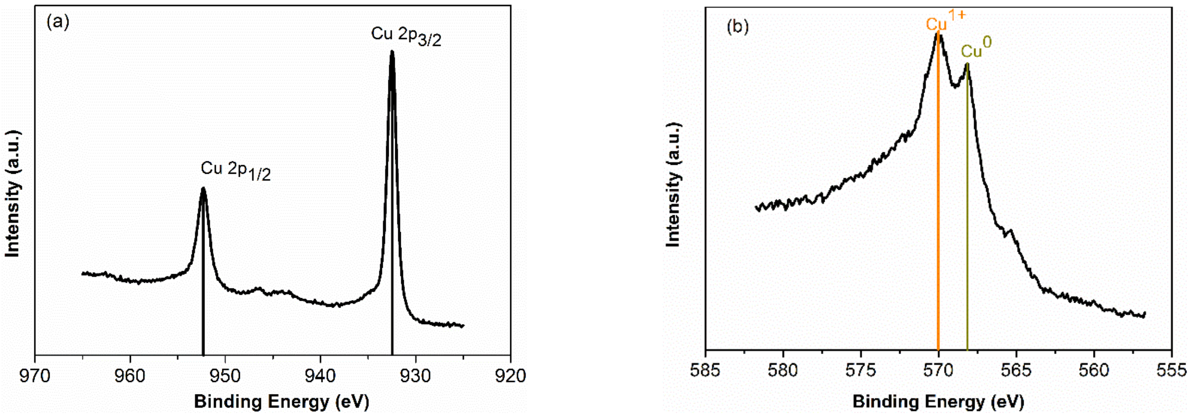

Figure 6. (a) Representative Cu X-ray photoelectron spectra; (b) Representative auger spectra for Cu electrodes deposited at −2 V with 45 seconds.

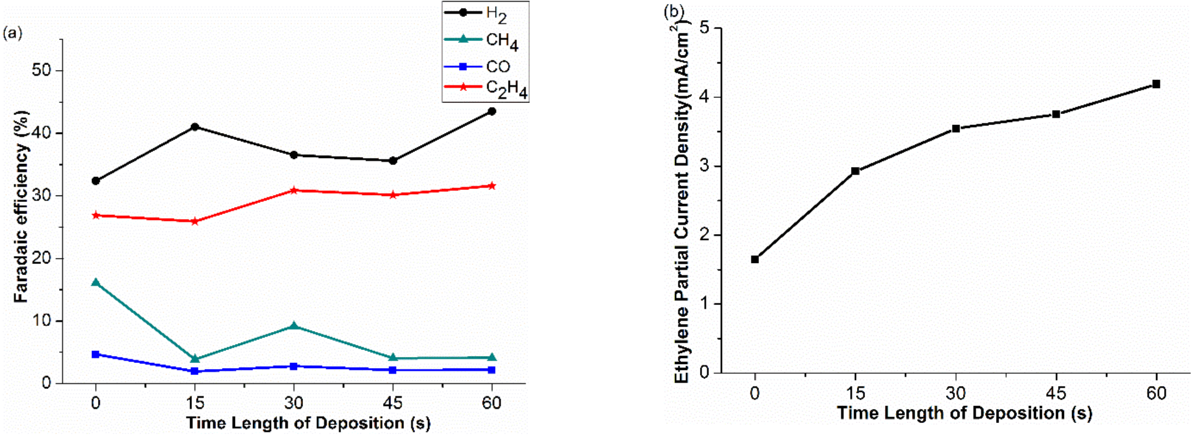

Figure 7. (a). Faradaic efficiency of gaseous products; (b) ethylene partial current density on different electrodes deposited under different time lengths of electrodeposition at −1.7 V vs Ag/AgCl in 0.1 M $KHCO_3$.

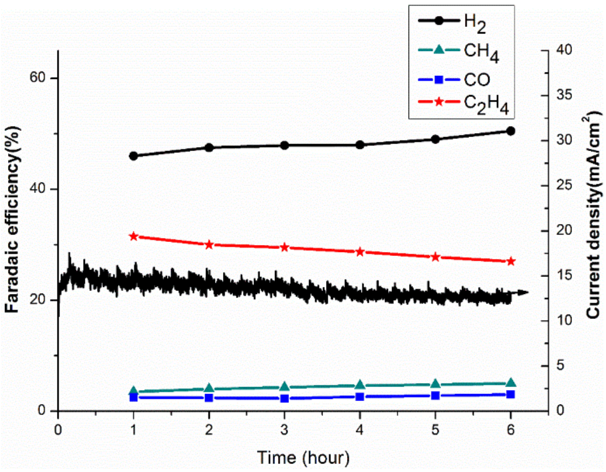

Figure 8. Six hours' stability performance on electrodeposited copper electrode over 60 seconds at −1.7 V vs.Ag/AgCl in 0.1 M $KHCO_3$.

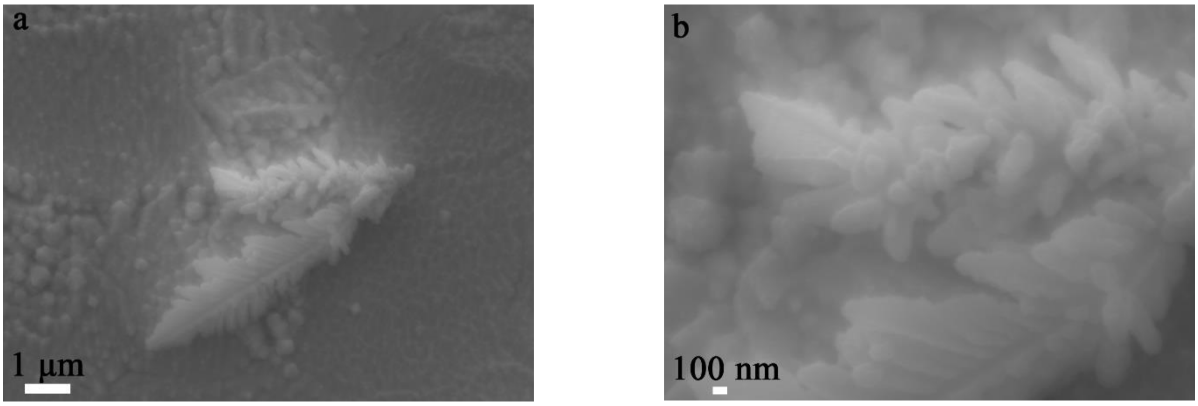

Figure 9. SEM images of electrodeposited copper electrode over 60 seconds after the electrochemical CO_2 reduction in 0.1 M $KHCO_3$ over 6 hours.

Figure 7 showed the relationship between the faradaic efficiency of gaseous products and the length of electrodeposition time at −1.7 V vs. Ag/AgCl. The faradaic efficiency for ethylene with the 15-second deposition electrode was essentially the same as the control sample, while longer lengths of deposition time increased the faradaic efficiency to ca. 32%. Compared to the control sample, hydrogen generation was also favored on the electrodeposited copper electrodes, while formation of methane and CO was suppressed. In addition, it was found that the partial current density for the formation of ethylene increased as the length of deposition time increased. Electrodeposited copper electrodes exhibited a fairly good catalytic stability and dendrites were still observed over the course of 6 hours. (Figure 8, 9)

Figure 10 showed the faradaic efficiency of the gaseous products on the electrodeposited copper over 60 seconds as a function of the applied potential. Faradaic efficiency of ethylene increased from 2% at −1.3 V to 32% at −1.7 V. Methane was not observed until −1.5 V. At the same time, faradaic efficiency of methane was lower than that of ethylene across the potential window. Faradaic efficiency of CO decreased as the overpotential increased. Relatively high faradaic efficiency of hydrogen (>40%) was observed across the potential window.

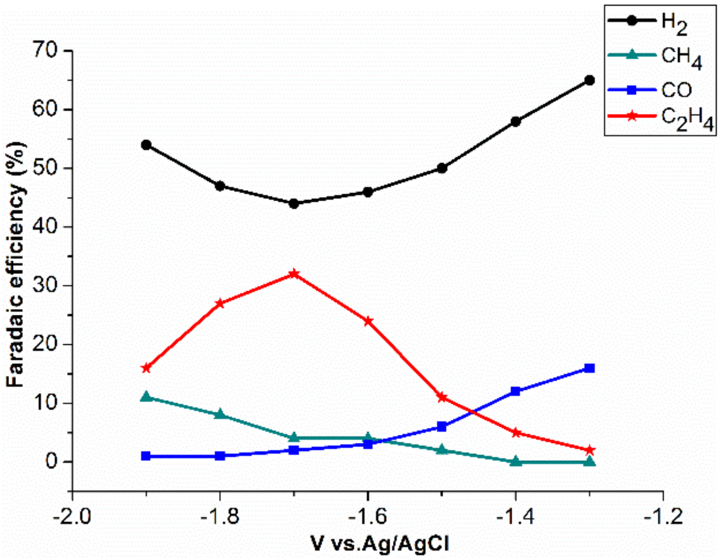

Figure 10. Faradaic efficiency of gaseous products on electrodeposited copper electrode over 60 seconds as a function of the applied potential in 0.1 M $KHCO_3$.

Table 3. Data for electrodeposited copper catalysts

Ethylene faradaic efficiency/%	Potential/ (V vs. Ag/AgCl)	Reference
32	−1.7	This work
<2%	−1.7	[20]
20%	−1.43	[23]
<15%	−1.9	[22]
~20%	−1.73	[12]

As can be seen from Table 3, the previously reported highest faradaic efficiency of ethylene using electrodeposited copper catalysts is ca. 20%, much lower than our system. The present work provides the first example that shows copper electrode prepared via electrodeposition, a method that can be scaled up conveniently, can lead to higher faradaic efficiency of ethylene than that of polycrystalline copper at the same overpotential.

There are several likely reasons for the improved faradaic efficiency of ethylene observed for the present systems. Electrochemical reduction of carbon dioxide to produce OH^- resulted in an increase of pH on the local surface of the electrode [26,27]. Compared to the control sample, electrodeposited dendritic structures increased the surface roughness of the electrode and thus the current density of the reaction, resulting in a more intense increase of local pH. The high local pH could promote the dimerization of CO, thereby enhancing the formation of ethylene [28-30]. Furthermore, the non-porous structures prepared via electrodeposition under acid-free conditions as the catalysts effectively avoided the further hydrogenation of ethylene to ethane, which presumably lowered the faradaic efficiency of ethylene by trapping ethylene in the electrochemically reductive porous electrode interface from the soft-template method [12,20,22,23]. On the other hand, it has been shown that the high-index stepped surface with low coordination sites led to higher selectivity for the formation of ethylene than the low-index surfaces [31].

4. CONCLUSIONS

In summary, we prepared copper electrodes with different microstructures via electrodeposition under acid-free conditions. The morphology and the crystal orientation of the deposited Cu material can be tuned via changing the length of electrodeposition time. In contrast to previous porous copper electrodes obtained via electrodeposition under acid conditions, the current dendritic materials resulted in improved faradaic efficiency of ethylene relative to polycrystalline copper electrode. Therefore, the nonporous, roughened surface might act together with the increased exposed (3 1 1) surfaces to increase the selectivity of C2 product and decrease the undesired over-reduction of ethylene to ethane for the present system. This work highlights the exquisite sensitivity for the formation of ethylene during the electrochemical reduction of carbon dioxide.

ACKNOWLEDGEMENTS
This work was financially supported by Shell-CAS Frontier Sciences Program (No. PT48809) from Shell and start-up funding from ShanghaiTech University.

References

1. M. Liu, T. Qin, Q. Zhang, C. Fang, Y. Fu, B.-L. Lin, *Sci. China: Chem.*, 58 (2015) 1524.
2. A. Chen, B.-L. Lin, *Joule*, 2 (2018) 594.
3. A. Goeppert, M. Czaun, J.P. Jones, G.K. Surya Prakash, G.A. Olah, *Chem. Soc. Rev.*, 43 (2014) 7995.
4. G.A. Olah, G.K. Prakash, A. Goeppert, *J. Am. Chem. Soc.*, 133 (2011) 12881.
5. D. Kim, K.K. Sakimoto, D. Hong, P. Yang, *Angew. Chem., Int. Ed*, 54 (2015) 3259.
6. Y. Hori, K. Kikuchi, A. Murata, S. Suzuki, *Chem. Lett.*, 15 (1986) 897.
7. K.P. Kuhl, E.R. Cave, D.N. Abram, T.F. Jaramillo, *Energy Environ. Sci.*, 5 (2012) 7050.
8. A. Loiudice, P. Lobaccaro, E.A. Kamali, T. Thao, B.H. Huang, J.W. Ager, R. Buonsanti, *Angew. Chem., Int. Ed.*, 55 (2016) 1.
9. H. Mistry, A.S. Varela, C.S. Bonifacio, I. Zegkinoglou, I. Sinev, Y.W. Choi, K. Kisslinger, E.A. Stach, J.C. Yang, P. Strasser, B.R. Cuenya, *Nat. Commun.*, 7 (2016) 12123.
10. D.A. Torelli, S.A. Francis, J.C. Crompton, A. Javier, J.R. Thompson, B.S. Brunschwig, M.P. Soriaga, N.S. Lewis, *ACS Catal.*, 6 (2016) 2100.
11. J. Wu, S. Ma, J. Sun, J.I. Gold, C. Tiwary, B. Kim, L. Zhu, N. Chopra, I.N. Odeh, R. Vajtai, A.Z. Yu, R. Luo, J. Lou, G. Ding, P.J. Kenis, P.M. Ajayan, *Nat. Commun.*, 7 (2016) 13869.
12. A. Dutta, M. Rahaman, M. Mohos, A. Zanetti, P. Broekmann, *ACS Catal.*, 7 (2017) 5431.
13. S. Lee, D. Kim, J. Lee, *Angew. Chem., Int. Ed.*, 127 (2015) 14914.
14. R. Kas, R. Kortlever, A. Milbrat, M.T.M. Koper, G. Mul, J. Baltrusaitis, *Phys. Chem. Chem. Phys.*, 16 (2014) 12194.
15. C.S. Chen, A.D. Handoko, J.H. Wan, L. Ma, D. Ren, B.S. Yeo, *Catal. Sci. Technol.*, 5 (2015) 161.
16. C.W. Li, M.W. Kanan, *J. Am. Chem. Soc.*, 134 (2012) 7231.
17. W. Tang, A.A. Peterson, A.S. Varela, Z.P. Jovanov, L. Bech, W.J. Durand, S. Dahl, J.K. Nøskov, I. Chorkendorff, *Phys. Chem. Chem. Phys.*, 14 (2012) 76.
18. B.J. Plowman, S.K. Bhargava, A.P. O'Mullane, *Analyst*, 136 (2011) 5107.
19. H.C. Shin, J. Dong, M. Liu, *Adv. Mater.*, 15 (2003) 1610.

20. S. Sen, D. Liu, G.T.R. Palmore, *ACS Catal.*, 4 (2014) 3091.
21. T.N. Huan, P. Simon, G. Rousse, I. Génois, V. Artero, M. Fontecave, *Chem. Sci.*, 8 (2017) 742.
22. M.R. Gonçalves, A. Gomes, J. Condeço, T.R.C. Fernandes, T. Pardal, C.A.C. Sequeira, J.B. Branco, *Electrochim. Acta*, 102 (2013) 388.
23. A. Dutta, M. Rahaman, N.C. Luedi, P. Broekmann, *ACS Catal.*, 6 (2016) 3804.
24. R. Qiu, H.G. Cha, H.B. Noh, Y.B. Shim, X.L. Zhang, R. Qiao, D. Zhang, Y.I. Kim, U. Pal, Y.S. Kang, *J. Phys. Chem. C*, 113 (2009) 15891.
25. D. Kim, S. Lee, J.D. Ocon, B. Jeong, J.K. Lee, J. Lee, *Phys. Chem. Chem. Phys.*, 17 (2015) 824.
26. Y. Hori, A. Murata, R. Takahashi, *J. Chem. Soc., Faraday Trans. 1, 85* (1989) 2309.
27. M. Ma, K. Djanashvili, W. A. Smith, *Angew. Chem., Int. Ed., 55* (2016) 6679.
28. K.J. Schouten, Z. Qin, E. P. Gallent, M.T. Koper, *J. Am. Chem. Soc.*, 134 (2012) 9864.
29. K.J.P. Schouten, E. P. Gallent, M. Koper, *J.Electroanal. Chem.*, 716 (2014) 53.
30. R. Kas, R. Kortlever, H. Yılmaz, M.T.M. Koper, G. Mul, *ChemElectroChem*, 2 (2015) 354.
31. Y. Hori, I. Takahashi, O. Koga, N. Hoshi, *J. Mol. Catal. A: Chem.*, 199 (2003) 39.